Preprints of the 20th World Congress
The International Federation of Automatic Control
Toulouse, France, July 9-14, 2017

Advanced computational design of shared tuned mass-inerter dampers for vibration control of adjacent multi-story structures ⋆

F. Palacios-Quiñonero * **J. Rubió-Massegú** * **J.M. Rossell** *
H.R. Karimi **

* *Department of Mathematics, Universitat Politècnica de Catalunya, Av. Bases de Manresa 61–73, 08242 Manresa, Barcelona, Spain (e-mail: {francisco.palacios, josep.rubio, josep.maria.rossell}@upc.edu).*
** *Politecnico di Milano, Department of Mechanical Engineering, via La Masa 1, 20156 Milan, Italy (e-mail: hamidreza.karimi@polimi.it)*

Abstract: Inerters are a novel type of mechanical actuation devices that are able to produce large inertial forces with a relatively small mass. Due to this property, inerters can provide an effective solution to the main drawbacks of tuned mass-dampers and, consequently, they are gaining an increasing relevance in the field of passive structural vibration control. In this paper, a computational design strategy for inerter-based vibration control schemes is presented. The proposed approach combines a computationally effective reduced-frequency H_∞ cost-function and a constrained global optimization solver to design different configurations of a shared tuned mass-inerter-damper system for the seismic protection of a multi-story two-building structure. To assess the effectiveness of the obtained configurations, the frequency characteristics and the seismic response of the interstory drifts and interbuilding approaches are investigated with positive results.

Keywords: inerters, structural vibration control, multi-structure systems, genetic algorithms, shared tuned mass-damper

1. INTRODUCTION

Protection of large buildings and civil structures against the damaging effects of external natural disturbances, such as wind gusts, earthquakes, or ocean waves is a research area of significant theoretical and technical interest. In the past few decades, a large number of active, passive and semi-active structural vibration control strategies has been proposed and, some of them, implemented in practice with positive results [Spencer and Nagarajaiah (2003); Ikeda (2009); Li and Huo (2010); Rubió-Massegú et al. (2012); Bakka and Karimi (2013)]. Passive vibration control systems (PVCS) are simple and robust, and do not require power supply. A good example of PVCS is the tuned mass-damper (TMD), which consists in a proper combination of elastic, damping and mass elements that are attached to the main structure to absorb and dissipate its vibrational energy. In order to provide a good level of vibrational mitigation, the TMD strategy requires the attached mass to be as large as possible. In the case of large structures, this fact makes the TMD a huge and massive device whose accommodation poses serious structural problems [Giaralis and Taflanidis (2016)].

Inerters are a new kind of passive elements in mechanical systems that are attracting increasing research attention in recent years. The ideal inerter is a massless two-terminal device that produces a resistant force of the form $F(t) = b\left(\ddot{x}_2(t) - \ddot{x}_1(t)\right)$, where $\ddot{x}_1(t)$ and $\ddot{x}_2(t)$ represent the inerter terminals' acceleration and b is a constant called *inertance*. A key feature of the actual inerter is that its inertance can be two or more orders of magnitude higher than its mass. As a consequence, light and compact devices that are able to develop large inertial forces can be seriously considered in practical applications [Smith (2002)]. This fact, and the two-terminal character of the inerter elements, naturally leads to explore new passive vibration control schemes, such as inerter-based multi-element distributed systems and more sophisticated spring-damper-inerter layouts [Chen et al. (2013); Lazar et al. (2014); Marian and Giaralis (2014)]. In this context, obtaining efficient tools to compute suitable values for the inertance, stiffness and damping coefficients appears as a central issue.

The objective of the present work is twofold: (i) to provide a proper computational design methodology for the new inerter-based vibration control schemes, and (ii) to demonstrate its effectiveness in a structural vibration control problem of moderate complexity and dimension. To meet the first goal, we have introduced an appropriate cost function $J(\theta)$, which is based on the discrete approximation of a restricted frequency-range H_∞ norm. This cost function provides a fast and meaningful evaluation of the vibrational cost associated to the parameter configuration θ, and makes it possible to obtain an optimal parameter configuration $\hat{\theta}$ by using standard tools for constrained global optimization. To address the second objective, the

⋆ Partially supported by the Spanish Ministry of Economy and Competitiveness under Grant DPI2015-64170-R/FEDER.

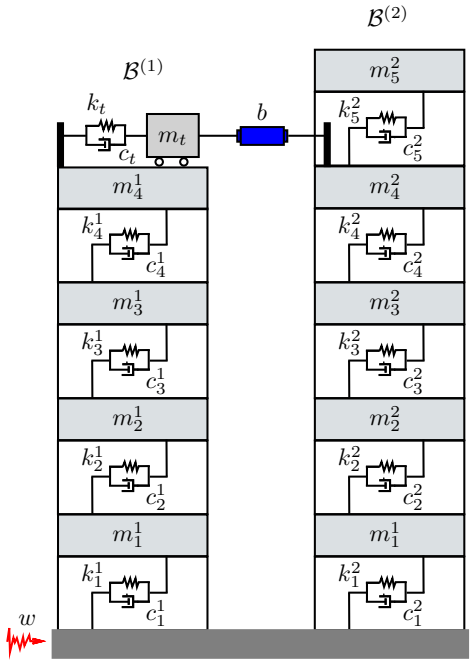

Fig. 1. Multi-story two-building system.

proposed approach has been applied in designing two different inerter-based vibration control schemes for the seismic protection of a multi-story two-building structure. To assess the effectiveness of the obtained optimal configurations, their frequency response characteristics have been investigated and a proper set of numerical simulations has been conducted using the full scale North–South El Centro 1940 seismic record as ground acceleration disturbance.

The rest of the paper is organized as follows: In Section 2, a mathematical model of the two-building structure is provided. The presented matrix formulation facilitates a clear and easy inclusion of the design parameters. In Section 3, the main ideas of the proposed computational design strategy are presented. In Section 4, the two inerter-based vibration control schemes are computed, and their corresponding frequency and seismic responses are investigated. Finally, some conclusions and future research directions are briefly discussed in Section 5.

2. TWO-BUILDING MATHEMATICAL MODEL

Let us consider the multi-story two-building system schematically shown in Fig. 1. The buildings' lateral motion can be described by the second-order model

$$\mathbf{M}\,\ddot{\mathbf{q}}(t) + \mathbf{C}\,\dot{\mathbf{q}}(t) + \mathbf{K}\,\mathbf{q}(t) = \mathbf{T}_w\,w(t),$$

where $\mathbf{q}(t)$ is the vector of displacements with respect to the ground, $\mathbf{M}$ is the generalized mass matrix, $\mathbf{C}$ is the damping matrix, $\mathbf{K}$ is the stiffness matrix, $\mathbf{T}_w$ is the disturbance input matrix and $w(t)$ is the ground acceleration disturbance. The vector of displacements can be written in the form

$$\mathbf{q}(t) = \begin{bmatrix} \mathbf{q}^{(1)}(t) \\ \mathbf{q}^{(2)}(t) \\ q_t(t) \end{bmatrix},$$

where

$$\mathbf{q}^{(1)}(t) = \left[q_1^1(t), \ldots, q_4^1(t)\right]^T,\ \mathbf{q}^{(2)}(t) = \left[q_1^2(t), \ldots, q_5^2(t)\right]^T,$$

$q_i^j(t)$ represents the displacement of the ith story in the building $\mathcal{B}^{(j)}$, and $q_t(t)$ is the displacement of the TMD placed at the top level of the building $\mathcal{B}^{(1)}$. The linking element between the TMD and the building $\mathcal{B}^{(2)}$ is an inerter with an inertance coefficient b, which produces a resistant force $F_b(t) = b\,(\ddot{q}_4^2 - \ddot{q}_t)$. The generalized mass matrix $\mathbf{M}$ has the following structure:

$$\mathbf{M} = \mathbf{M}_0 + b \begin{bmatrix} [\mathbf{0}]_{4\times4} & [\mathbf{0}]_{4\times5} & [\mathbf{0}]_{4\times1} \\ [\mathbf{0}]_{5\times4} & \mathrm{diag}(\mathbf{p}_2) & -\mathbf{p}_2 \\ [\mathbf{0}]_{1\times4} & -\mathbf{p}_2^T & 1 \end{bmatrix},$$

where $\mathbf{M}_0 = \mathrm{diag}(\mathbf{M}^{(1)}, \mathbf{M}^{(2)}, m_t)$ is the mass matrix corresponding to null inertance, $\mathbf{M}^{(1)} = \mathrm{diag}(m_1^1, \ldots, m_4^1)$ and $\mathbf{M}^{(2)} = \mathrm{diag}(m_1^2, \ldots, m_5^2)$ are the mass matrices of the buildings $\mathcal{B}^{(1)}$ and $\mathcal{B}^{(2)}$, respectively, m_i^j is the mass of the ith story in the building $\mathcal{B}^{(j)}$, m_t is the TMD mass, $[\mathbf{0}]_{r\times s}$ is a zero matrix of dimensions $r \times s$ and the placement vector $\mathbf{p}_2 = (0,0,0,1,0)^T$ indicates the story level of the building $\mathcal{B}^{(2)}$ where the inerter element is located. The stiffness matrix has the following structure:

$$\mathbf{K} = \mathrm{diag}(\mathbf{K}^{(1)}, \mathbf{K}^{(2)}, 0) + k_t \begin{bmatrix} \mathbf{p}_1\mathbf{p}_1^T & [\mathbf{0}]_{4\times5} & -\mathbf{p}_1 \\ [\mathbf{0}]_{5\times4} & [\mathbf{0}]_{5\times5} & [\mathbf{0}]_{5\times1} \\ -\mathbf{p}_1^T & [\mathbf{0}]_{1\times5} & 1 \end{bmatrix},$$

where

$$\mathbf{K}^{(1)} = \begin{bmatrix} k_1^1 + k_2^1 & -k_2^1 & 0 & 0 \\ -k_2^1 & k_2^1 + k_3^1 & -k_3^1 & 0 \\ 0 & -k_3^1 & k_3^1 + k_4^1 & -k_4^1 \\ 0 & 0 & -k_4^1 & k_4^1 \end{bmatrix},$$

$$\mathbf{K}^{(2)} = \begin{bmatrix} k_1^2 + k_2^2 & -k_2^2 & 0 & 0 & 0 \\ -k_2^2 & k_2^2 + k_3^2 & -k_3^2 & 0 & 0 \\ 0 & -k_3^2 & k_3^2 + k_4^2 & -k_4^2 & 0 \\ 0 & 0 & -k_4^2 & k_4^2 + k_5^2 & -k_5^2 \\ 0 & 0 & 0 & -k_5^2 & k_5^2 \end{bmatrix},$$

are the stiffness matrices of the buildings $\mathcal{B}^{(1)}$ and $\mathcal{B}^{(2)}$, respectively, k_i^j is the stiffness coefficient of the ith story in the building $\mathcal{B}^{(j)}$, k_t is the TMD stiffness and the placement vector $\mathbf{p}_1 = (0,0,0,1)^T$ indicates the story level of the building $\mathcal{B}^{(1)}$ where the TMD is located. The damping matrix has an analogous structure

$$\mathbf{C} = \mathrm{diag}(\mathbf{C}^{(1)}, \mathbf{C}^{(2)}, 0) + c_t \begin{bmatrix} \mathbf{p}_1\mathbf{p}_1^T & [\mathbf{0}]_{4\times5} & -\mathbf{p}_1 \\ [\mathbf{0}]_{5\times4} & [\mathbf{0}]_{5\times5} & [\mathbf{0}]_{5\times1} \\ -\mathbf{p}_1^T & [\mathbf{0}]_{1\times5} & 1 \end{bmatrix},$$

where c_t is the TMD damping and $\mathbf{C}^{(j)}$ is the damping matrix of the building $\mathcal{B}^{(j)}$. When the damping coefficients are known, the matrix $\mathbf{C}^{(j)}$ can be obtained by replacing the stiffness coefficients k_i^j in $\mathbf{K}^{(j)}$ by the corresponding damping coefficients c_i^j. Frequently, however, the values of the damping coefficients cannot be properly determined and the matrices $\mathbf{C}^{(j)}$ are computed using other methods [Chopra (2007)]. Finally, the disturbance input matrix can be written as

$$\mathbf{T}_w = -\mathbf{M}_0\,[\mathbf{1}]_{10\times1},$$

where $[\mathbf{1}]_{10\times1}$ is a column vector with all its entries equal to 1. By considering the state vector

$$\mathbf{x}(t) = \begin{bmatrix} \mathbf{q}(t) \\ \dot{\mathbf{q}}(t) \end{bmatrix},$$

Table 1. Buildings mass and stiffness coefficient values

	building $\mathcal{B}^{(1)}$				building $\mathcal{B}^{(2)}$				
story	1	2	3	4	1	2	3	4	5
mass ($\times 10^5$ Kg)	2.152	2.092	2.070	2.661	2.152	2.092	2.070	2.048	2.661
stiffness ($\times 10^8$ N/m)	1.470	1.130	0.990	0.840	1.470	1.130	0.990	0.890	0.840

we obtain the first-order state-space model

$$\dot{\mathbf{x}}(t) = \mathbf{A}\,\mathbf{x}(t) + \mathbf{B}\,w(t),$$

with system matrices

$$\mathbf{A} = \begin{bmatrix} [\mathbf{0}]_{10\times 10} & \mathbf{I}_{10} \\ -\mathbf{M}^{-1}\mathbf{K} & -\mathbf{M}^{-1}\mathbf{C} \end{bmatrix},\ \mathbf{B} = \begin{bmatrix} [\mathbf{0}]_{10\times 1} \\ -\mathbf{M}^{-1}\mathbf{M}_0[\mathbf{1}]_{10\times 1} \end{bmatrix},$$

where $\mathbf{I}_n$ denotes the identity matrix of order n.

3. DESIGN PROCEDURE

In this section, the main ideas of the proposed computational design strategy are discussed. An application of these ideas using a global optimization solver based on the genetic algorithm approach is presented in the next section.

In order to describe the overall vibrational response of the adjacent buildings, we consider two different sets of output variables: *interstory drifts* and *interbuilding approaches* [Palacios-Quiñonero et al. (2012, 2014)]. The interstory drifts are the relative displacements between consecutive stories of the same building, and can be defined as

$$\begin{cases} r_1^j(t) = q_1^j(t), \\ r_i^j(t) = q_i^j(t) - q_{i-1}^j(t),\ 1 < i \leq n_j, \end{cases}$$

where n_j represents the number of stories of the building $\mathcal{B}^{(j)}$. The overall vector of interstory drifts can be written in the form

$$\mathbf{r}(t) = \begin{bmatrix} \mathbf{r}^{(1)}(t) \\ \mathbf{r}^{(2)}(t) \end{bmatrix}$$

where $\mathbf{r}^{(j)}(t) = \left[r_1^j(t), \ldots, r_{n_j}^j(t)\right]^T$ is the vector of interstory drifts of the building $\mathcal{B}^{(j)}$. By considering the state vector $\mathbf{x}(t)$, the overall vector of interstory drifts can be computed as

$$\mathbf{r}(t) = \mathbf{C}_r\,\mathbf{x}(t),$$

where the output matrix has the form

$$\mathbf{C}_r = \left[\ \tilde{\mathbf{C}}_r\ [\mathbf{0}]_{9\times 11}\ \right],$$

with

$$\tilde{\mathbf{C}}_r = \begin{bmatrix} \mathbf{C}_r^{(1)} & [\mathbf{0}]_{4\times 5} \\ [\mathbf{0}]_{5\times 4} & \mathbf{C}_r^{(2)} \end{bmatrix},$$

$$\mathbf{C}_r^{(1)} = \begin{bmatrix} 1 & 0 & 0 & 0 \\ -1 & 1 & 0 & 0 \\ 0 & -1 & 1 & 0 \\ 0 & 0 & -1 & 1 \end{bmatrix},\ \mathbf{C}_r^{(2)} = \begin{bmatrix} 1 & 0 & 0 & 0 & 0 \\ -1 & 1 & 0 & 0 & 0 \\ 0 & -1 & 1 & 0 & 0 \\ 0 & 0 & -1 & 1 & 0 \\ 0 & 0 & 0 & -1 & 1 \end{bmatrix}.$$

The interbuilding approaches

$$a_i(t) = -\left(q_i^2(t) - q_i^1(t)\right),\ 1 \leq i \leq \min(n_1, n_2),$$

describe the approaching between the stories located at the same level in adjacent buildings. For our particular two-building system, the vector of interbuilding approaches $\mathbf{a}(t) = [a_1(t), \ldots, a_4(t)]^T$, can be computed as

$$\mathbf{a}(t) = \mathbf{C}_a\,\mathbf{x}(t),$$

Table 2. Buildings natural frequencies

	Frequency (Hz)				
Building $\mathcal{B}^{(1)}$	1.2404	3.4161	5.3160	6.7272	
Building $\mathcal{B}^{(2)}$	1.0082	2.8246	4.4929	5.7974	6.7735

with the output matrix

$$\mathbf{C}_a = \left[\ \mathbf{I}_4\ -\mathbf{I}_4\ [\mathbf{0}]_{4\times 12}\ \right]. \tag{1}$$

In the present work, the buildings mass, damping and stiffness are assumed to be known, and the design objective is to determine suitable values of the TMD parameters m_t, c_t, k_t, and the inertance b. Although we are interested in reducing both the interstory drifts and interbuilding approaches, it should be noted that reduced interstory drifts always lead to small interbuilding approaches. In contrast, demanding small interbuilding approaches can produce large interstory drifts. Considering this fact, the design procedure is focused on reducing the interstory drift response. Accordingly, we consider the system

$$\mathcal{S}_\theta : \begin{cases} \dot{\mathbf{x}}(t) = \mathbf{A}_\theta\,\mathbf{x}(t) + \mathbf{B}_\theta\,w(t), \\ \mathbf{z}(t) = \mathbf{C}_r\,\mathbf{x}(t), \end{cases}$$

where the system matrices $\mathbf{A}_\theta$ and $\mathbf{B}_\theta$ are functions of the parameter vector $\theta = (m_t, c_t, k_t, b)$. The basic idea of the design procedure is simple, it consists in computing an optimal parameter vector $\hat{\theta}$ by solving a constrained optimization problem

$$\mathcal{P} : \begin{cases} \min J(\theta), \\ \text{subject to } \theta \in \Theta_c, \end{cases} \tag{2}$$

where $J(\theta)$ is an appropriate objective function and Θ_c is a suitable parameter domain. In order to make it possible to use standard tools for constrained global optimization, the objective function must be able to make a fast and meaningful evaluation of the vibrational cost associated to the parameter configuration θ. To meet these requirements, we define the objective function $J(\theta)$ as the discrete approximation of a restricted frequency-range H_∞ norm. Specifically, we first consider the system H_∞ norm

$$\gamma(\theta) = \sup_{0<\|w\|_2<\infty} \frac{\|\mathbf{z}\|_2}{\|w\|_2},$$

which describes the worst-case energy-gain from the external disturbance $w(t)$ to the controlled output $\mathbf{z}(t)$. This norm can be computed in the frequency domain by using the transfer function

$$\mathbf{T}_\theta(s) = \mathbf{C}_r(s\mathbf{I} - \mathbf{A}_\theta)^{-1}\mathbf{B}_\theta$$

and solving the optimization problem

$$\gamma(\theta) = \sup_{f\in\mathbb{R}} \left\{\sigma_{\max}\left[\mathbf{T}_\theta(2\pi j f)\right]\right\},$$

where $j = \sqrt{-1}$, f is the frequency in Hz and $\sigma_{\max}[\cdot]$ denotes the maximum singular value. Next, to reduce the computational burden without degrading the quality of the vibrational cost evaluation, we select a suitable frequency

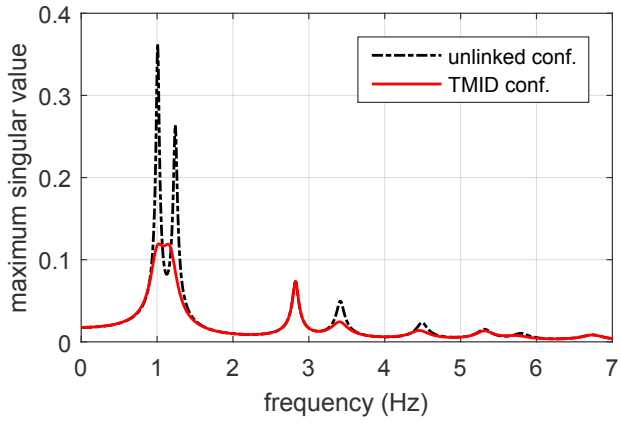

Fig. 2. Interstory-drifts frequency response for the TMID configuration.

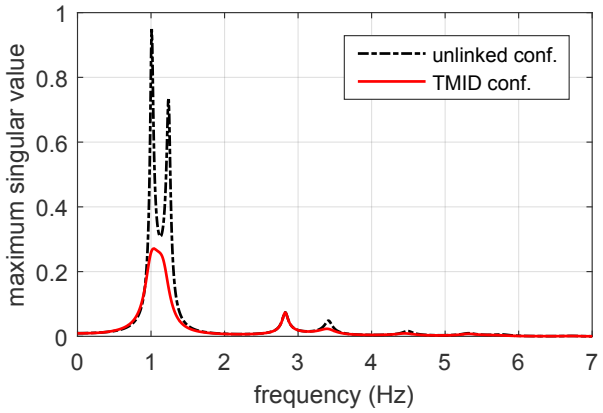

Fig. 3. Interbuilding-approaches frequency response for the TMID configuration.

range F_c, for example, a small interval that contains the buildings main frequencies, and consider the constrained γ-value

$$\gamma_c(\theta) = \max_{f \in F_c} \{\sigma_{\max}[\mathbf{T}_\theta(2\pi j f)]\}.$$

Finally, to obtain a fast estimate of $\gamma_c(\theta)$, we make a direct grid search in the frequency range F_c and compute

$$J(\theta) = \gamma_c^*(\theta) = \max_{i=1,\ldots,n_\gamma} \{\sigma_{\max}[\mathbf{T}_\theta(2\pi j f_i)]\},$$

where $f_1, \ldots, f_{n_\gamma}$ is a sequence of n_γ equally spaced frequency values in F_c.

4. NUMERICAL RESULTS

4.1 TMID and TID configurations

In this section, the proposed design strategy is applied to compute suitable parameter values for two different configurations: (i) a tuned mass-inerter damper (TMID) setup that combines the actions of the TMD and the inerter element, and (ii) a tuned inerter-damper (TID) configuration, which acts as a massless vibration absorber. The designs and numerical simulations are conducted using the buildings parameters collected in Table 1. These mass and stiffness values are similar to those used in Kurata et al. (1999). The buildings damping matrices (in Ns/m) are the following:

$$\mathbf{C}^{(1)} = 10^5 \times \begin{bmatrix} 2.6450 & -0.9034 & 0 & 0 \\ -0.9034 & 2.2455 & -0.7915 & 0 \\ 0 & -0.7915 & 2.0078 & -0.6715 \\ 0 & 0 & -0.6715 & 1.3719 \end{bmatrix},$$

$$\mathbf{C}^{(2)} = 10^5 \times \begin{bmatrix} 2.6017 & -0.9244 & 0 & 0 & 0 \\ -0.9244 & 2.1958 & -0.8099 & 0 & 0 \\ 0 & -0.8099 & 1.9946 & -0.7281 & 0 \\ 0 & 0 & -0.7281 & 1.8670 & -0.6872 \\ 0 & 0 & 0 & -0.6872 & 1.2741 \end{bmatrix},$$

which have been computed as Rayleigh damping matrices with a 2% of relative damping on the first and last modes [Chopra (2007)]. The natural frequencies corresponding to the unlinked buildings are presented in Table 2. Considering the values of the main frequencies, we select the frequency range $F_c = [0.85\,\text{Hz}, 1.40\,\text{Hz}]$ to compute the constrained gamma value $\gamma_c(\theta)$, which is approximated by using a uniform grid of $n_\gamma = 40$ points. The optimization problem $\mathcal{P}$ given in (2) is solved with the function `ga()` included in the Matlab Global Optimization Toolbox. This function provides an implementation of the genetic algorithm and allows defining lower and upper limits for the optimization variables. The parameter domain Θ_c is defined by considering an initial estimate $\tilde{\theta} = \left(\tilde{m}_t, \tilde{c}_t, \tilde{k}_t, \tilde{b}\right)$ and setting lower and upper variables bounds of the following form:

$$\theta_l = \left(\alpha_1 \tilde{m}_t, \alpha_2 \tilde{c}_t, \alpha_3 \tilde{k}_t, \alpha_4 \tilde{b}\right),\ \theta_u = \left(\beta_1 \tilde{m}_t, \beta_2 \tilde{c}_t, \beta_3 \tilde{k}_t, \beta_4 \tilde{b}\right).$$

For the TMID configuration, we set the initial values $\tilde{m}_t = 2 \times 10^4$ Kg, $\tilde{c}_t = 5 \times 10^5$ Ns/m, $\tilde{k}_t = 5 \times 10^5$ N/m and $\tilde{b} = 2 \times 10^5$ Kg. The selected TMD mass is about a 10% of the upper story mass and the selected inertance is similar to the full story mass. The optimization constraints are defined with the following coefficients: $\alpha_1 = 0.1$, $\alpha_2 = \alpha_3 = 0.01$, $\alpha_4 = 0.1$ and $\beta_1 = 1.2$, $\beta_2 = \beta_3 = 10$, $\beta_4 = 1.2$. This choice avoids negative values of the optimization variables, allows a variation of three orders of magnitude in the damping and stiffness coefficients, and restricts the mass and inertance values to small variations around the nominal values. The solver options `PolulationSize` and `TolFun` are set to 75 and 10^{-5}, respectively, and the default values are used for all the other options. After 57 iterations, the optimization process produces the parameter configuration $\hat{m}_t = 8.005 \times 10^3$ Kg, $\hat{c}_t = 5.721 \times 10^5$ Ns/m, $\hat{k}_t = 1.201 \times 10^6$ N/m, $\hat{b} = 1.150 \times 10^5$ Kg and the optimal cost $\hat{J} = 0.1192$. The required number of objective function evaluations is 4350, and the total computation time is 13.97 seconds.

For the TID configuration, we set the initial values: $\tilde{m}'_t = 1 \times 10^0$ Kg, $\tilde{c}'_t = 5 \times 10^3$ Ns/m, $\tilde{k}'_t = 5 \times 10^6$ N/m, and $\tilde{b}' = 5 \times 10^4$ Kg. In this second case, the aim is to obtain a massless vibration absorber by enforcing a pure inerter configuration with low damping and large stiffness. Running the optimization process with the same set of constraints and options, we obtain the following parameter values: $\hat{m}'_t = 1.159$ Kg, $\hat{c}'_t = 3.836 \times 10^4$ Ns/m, $\hat{k}'_t = 9.884 \times 10^5$ N/m, $\hat{b}' = 2.146 \times 10^4$ Kg, and the optimal cost $\hat{J}' = 0.1241$. In this second design, the number of iterations is 53, the count of function evaluations is 3900, and the total computation time is 12.58 seconds.

The frequency characteristics of the interstory drifts response corresponding to the TMID configuration are displayed in Fig. 2, where the solid red line presents the maximum singular values of the transfer function $\mathbf{T}_{\hat{\theta}}(s)$.

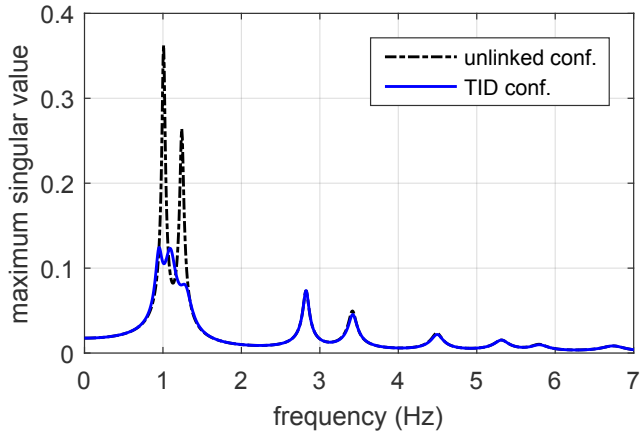

Fig. 4. Interstory-drifts frequency response for the TID configuration.

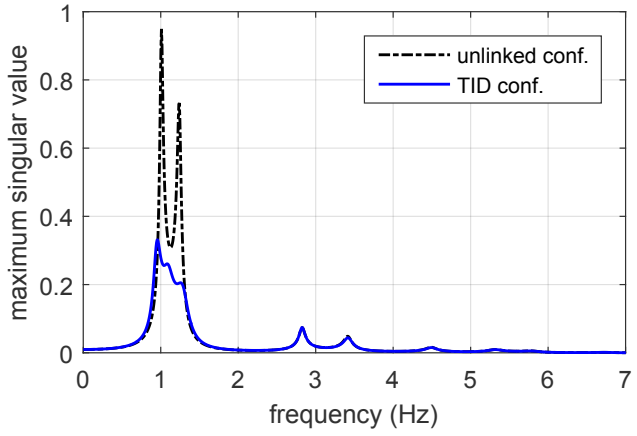

Fig. 5. Interbuilding-approaches frequency response for the TID configuration.

The dash-dotted black line shows the frequency response of the unlinked buildings, which has been taken as a natural reference. The two large peaks in the unlinked response are associated to the buildings' dominant frequencies and the peak value in the TMID configuration corresponds to the obtained optimal value $\hat{J}=0.1192$. The frequency characteristics of the interbuilding approaches response are presented in Fig. 3. In this case, the response corresponding to the TMID configuration (solid red line) has been computed using the transfer function from the external disturbance $w(t)$ to the approaches vector $\mathbf{a}(t)$

$$\tilde{\mathbf{T}}_{\hat{\theta}}(s) = \mathbf{C}_a(s\mathbf{I} - \mathbf{A}_{\hat{\theta}})^{-1}\mathbf{B}_{\hat{\theta}},$$

where $\mathbf{C}_a$ is the approaches output-matrix defined in (1). For the TID configuration, the frequency characteristics of the interstory drifts and interbuilding approaches response are presented by the solid blue line in Fig. 4 and Fig. 5, respectively. In an overall inspection of the plots, it can be appreciated that both configurations produce a significant reduction of the main frequency peaks. A closer look reveals that the reduction level is very similar in the interstory drift response, and that a slightly better performance is attained by the TMID configuration in the interbuilding approaches response. This configuration also produces an appreciable reduction in some of the secondary frequency peaks.

Remark. All the computations have been carried out using Matlab© R2015b on a regular laptop with an Intel© Core™ i7-2640M processor at 2.80 GHz.

4.2 Seismic response

In this section, numerical simulations are conducted to demonstrate the seismic response of the two-building system for the obtained TMID and TID configurations. The full scale *North–South El Centro 1940* seismic record is taken as ground acceleration disturbance (see Fig. 6), and the interbuilding approaches $\mathbf{a}(t)$ together with the buildings interstory drifts $\mathbf{r}^{(1)}(t)$ and $\mathbf{r}^{(2)}(t)$ are computed as output variables.

The peak-values of the interbuilding approaches are displayed in Fig. 7, where the red line with circles corresponds to the TMID configuration, the blue line with triangles represents the TID configuration and the black line with

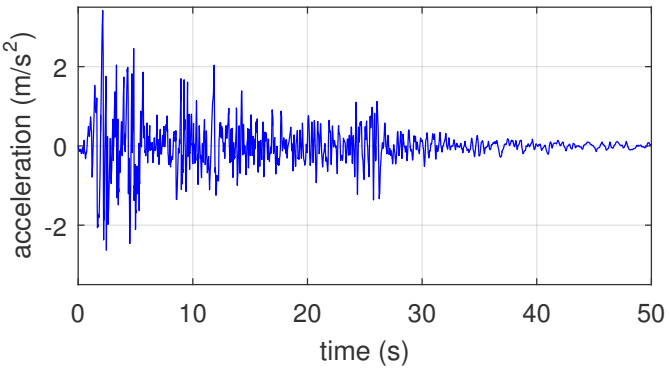

Fig. 6. Full scale North–South El Centro 1940 seismic record.

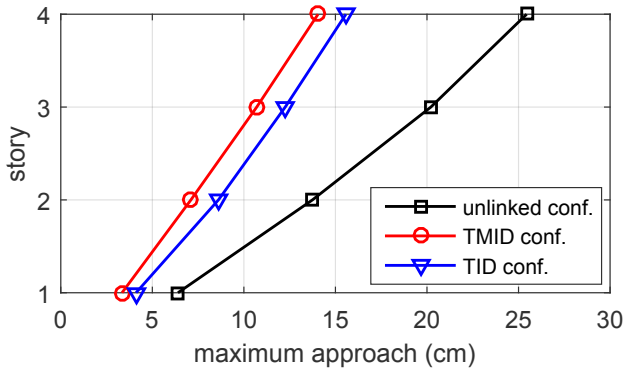

Fig. 7. Interbuilding approaches peak-values.

rectangles shows the response of the unlinked buildings. The maximum absolute interstory drifts peak-values corresponding to the buildings $\mathcal{B}^{(1)}$ and $\mathcal{B}^{(2)}$ are presented in Fig. 8 and Fig. 9, respectively, using the same symbols and colors. A quick inspection of the graphics shows that a similar reduction in the peak-values seismic response is attained by the proposed TMID and TID configurations, which produce a reduction of about 50% in the interbuilding approaches peaks-values, and around a 20% of reduction in the interstory drift peak-values of the lower stories in both buildings. The effectiveness in reducing the interstory drifts peak-values decreases in the upper stories, and is practically null at the top level. A slightly

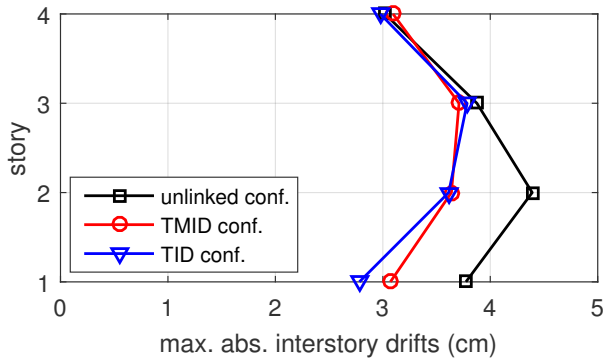

Fig. 8. Interstory drifts peak-values in building $\mathcal{B}^{(1)}$.

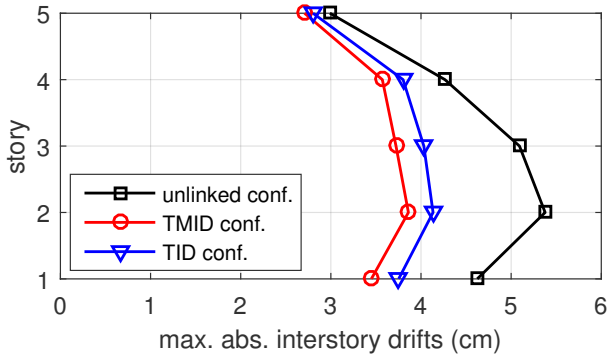

Fig. 9. Interstory drifts peak-values in building $\mathcal{B}^{(2)}$.

better performance is obtained by the TMID configuration, which is consistent with the information provided by the frequency-response plots. However, it should be highlighted that the inertance coefficient of an inerter element can be several orders of magnitude larger than its actual mass and, consequently, the response obtained by the TID configuration corresponds to a passive vibration control system with practically negligible mass.

Remark. To avoid the modeling complexity of interbuilding impacts, the seismic responses have been computed assuming that the interbuilding separation is large enough to avoid collisions. In this case, the maximum values of the interbuilding approaches can be understood as lower bounds of *safe interbuilding separation*. Looking at the plots in Fig. 7, it can be appreciated that an interbuilding separation of 16 cm can be considered safe for the proposed TMID and TID configurations. In contrast, a separation of 25 cm would have produced interbuilding collisions in the unlinked configuration.

5. CONCLUSIONS AND FUTURE DIRECTIONS

In this work, a computational strategy for the optimal design of passive vibration control systems has been presented. In addition to the typical elastic, damping and mass elements, the proposed approach allows including the novel inerter elements, which make it possible designing vibration absorber systems with a practically negligible mass. To illustrate the main ideas, two different tuned mass-inerter-damper configurations have been designed for the seismic protection of a multi-story two-building structure with positive results. Future lines of research include applying the proposed design methodology to obtain a suitable tuning of complex configurations, such as inerter-based multi-element distributed systems and more sophisticated spring-damper-inerter layouts.

REFERENCES

Bakka, T. and Karimi, H. (2013). H_∞ static output-feedback control design with constrained information for offshore wind turbine system. *Journal of the Franklin Institute*, 350(8), 2244–2260.

Chen, M., Wang, K., Zou, Y., and Lam, J. (2013). Realization of a special class of admittances with one damper and one inerter for mechanical control. *IEEE Transactions on Automatic Control*, 58(7), 1841–1846.

Chopra, A. (2007). *Dynamics of Structures. Theory and Applications to Earthquake Engineering*. Prentice Hall, Upper Saddle River, New Jersey, USA, 3rd edition.

Giaralis, A. and Taflanidis, A. (2016). Robust reliability-based design of seismically excited tuned mass-damper-inerter (TMDI) equipped MDOF structures with uncertain properties. In *6th European Conference on Structural Control EACS 2016*, Paper No. 150, 1–12. Sheffield, England.

Ikeda, Y. (2009). Active and semi-active vibration control of buildings in Japan - practical applications and verification. *Structural Control and Health Monitoring*, 16(7-8), 703–723.

Kurata, N., Kobori, T., Takahashi, M., Niwa, N., and Midorikawa, H. (1999). Actual seismic response controlled building with semi-active damper system. *Earthquake Engineering and Structural Dynamics*, 28(11), 1427–1447.

Lazar, I., Neild, S., and Wagg, D. (2014). Using an inerter-based device for structural vibration suppression. *Earthquake Engineering and Structural Dynamics*, 43(8), 1129–1147.

Li, H. and Huo, L. (2010). Advances in structural control in civil engineering in China. *Mathematical Problems in Engineering*, Article ID 936081, 1–23.

Marian, L. and Giaralis, A. (2014). Optimal design of a novel tuned mass-damper-inerter (TMDI) passive vibration control configuration for stochastically support-excited structural systems. *Probabilistic Engineering Mechanics*, 38, 156–164.

Palacios-Quiñonero, F., Rubió-Massegú, J., Rossell, J., and Karimi, H. (2012). Semiactive-passive structural vibration control strategy for adjacent structures under seismic excitation. *Journal of the Franklin Institute*, 349(10), 3003–3026.

Palacios-Quiñonero, F., Rubió-Massegú, J., Rossell, J., and Karimi, H. (2014). Vibration control for adjacent structures using local state information. *Mechatronics*, 24(4), 336–344.

Rubió-Massegú, J., Palacios-Quiñonero, F., and Rossell, J. (2012). Decentralized static output-feedback H_∞ controller design for buildings under seismic excitation. *Earthquake Engineering and Structural Dynamics*, 41(7), 1199–1205.

Smith, M. (2002). Synthesis of mechanical networks: The inerter. *IEEE Transactions on Automatic Control*, 47(10), 1648–1662.

Spencer, B. and Nagarajaiah, S. (2003). State of the art of structural control. *Journal of Structural Engineering*, 129(7), 845–856.